Comparison of electronic effects of β-aryl substituents on optical and electrochemical properties of 5,15-diazaporphyrin π-systems

Satoshi Omomo[a], Ko Furukawa[b], Haruyuki Nakano[c] and Yoshihiro Matano*[d◊]

[a] *Department of Fundamental Sciences, Graduate School of Science and Technology, Niigata University, Nishi-ku, Niigata 950-2181, Japan*

[b] *Center for Instrumental Analysis, Institute for Research Promotion, Niigata University, Nishi-ku, Niigata 950-2181, Japan*

[c] *Department of Chemistry, Graduate School of Sciences, Kyushu University, Fukuoka 812-8581, Japan*

[d] *Department of Chemistry, Faculty of Science, Niigata University, Nishi-ku, Niigata 950-2181, Japan*

Dedicated to Professor Nagao Kobayashi on the occasion of his 65th birthday

ABSTRACT: The syntheses and optical/electrochemical properties of 3-aryl-10,20-dimesityl-5,15-diazaporphyrin-metal complexes (MDAPs; mesityl = 2,4,6-trimethylphenyl; M = Ni, Zn) are reported. Treatment of 3-bromo-MDAPs with arylboronic acids in the presence of a Pd catalyst and a bulky phosphine ligand in a dioxane-water mixed solvent afforded the corresponding 3-aryl-MDAPs in moderate to good yields. X-ray crystallographic analysis of p-EtO$_2$CC$_6$H$_4$-NiDAP showed that the β-aryl group was tilted toward the NiDAP ring, with a dihedral angle of 21.7°. In the UV-visible absorption spectra, all the Ar-MDAPs showed intense Q-bands attributable to HOMO-to-LUMO transitions. The *para* substituents were found to influence the HOMO energies, which eventually resulted in fine tuning of the HOMO–LUMO gaps of the diazaporphyrin chromophores. It is worth noting that the p-Ph$_2$NC$_6$H$_4$-ZnDAP showed broad absorption and emission bands in the visible-near-infrared regions. The large Stokes shifts and their linear solvation energy relationships *vs.* orientation polarizability show that this Ph$_2$N-substituted derivative has intrinsically high charge transfer from the triphenylamine (donor) to the ZnDAP (acceptor) unit. These experimental observations were supported by theoretical calculations for model Ar-ZnDAP compounds. These results confirm that the introduction of a highly electron-donating aryl group at the peripheral β-carbon is a promising strategy for enhancing the light-harvesting and light-emitting abilities of diazaporphyrin-based π-systems in the visible-near-infrared regions.

KEYWORDS: diazaporphyrin, Suzuki–Miyaura coupling, π-conjugation, charge-transfer interaction.

INTRODUCTION

Metal complexes of 5,15-diazaporphyrin have D_{2h} symmetry, and their highest occupied molecular orbitals (HOMOs) and lowest unoccupied molecular orbitals (LUMOs) are nondegenerate [1, 2]. Because of these intrinsic properties, diazaporphyrins show intense and red-shifted Q-bands [3–6], and some derivatives have been investigated as potential sensitizers for use in photodynamic therapy [7], dye-sensitized solar cells [8], optical oxygen-sensing [9], and artificial photosynthesis [10]. However, guidelines for the molecular design of diazaporphyrin-based functional dyes that absorb both visible and near-infrared (NIR) light have not been yet established, because chemical functionalizations of the peripheral carbons with π-conjugative groups have

---

◊ SPP full member in good standing

*Correspondence to: Yoshihiro Matano, email: matano@chem. sc.niigata-u.ac.jp, tel: +81 25-262-7734, fax: +81 25-262-7734

not been studied in detail. Recently, Shinokubo *et al.* [11] and our group [12] independently reported the first synthesis of β-unsubstituted 10,20-dimesityl-5,15-diazaporphyrin-metal complexes (MDAPs; mesityl = 2,4,6-trimethylphenyl; M = Ni, Cu) **1M** (Chart 1), using metal-templated cyclizations of dichloro- or dibromo-dipyrrin-metal complexes with NaN_3 or CuN_3 [13]. We also established synthetic routes to other β-unsubstituted MDAPs **1M** (M = Zn, Pb, Pd, Pt) and used **1Ni**, **1Cu**, and **1Zn** as starting materials for β-functionalized MDAP derivatives [12, 14]. Our strategy for the peripheral functionalizations of MDAPs is based on cross-coupling reactions of 3-bromo-MDAPs **2M** (Br-MDAPs; M = Ni, Cu, Zn, Chart 1), which are readily obtained by regioselective bromination of **1M** with *N*-bromo-succinimide (NBS) [8, 12]. For example, covalently linked MDAP dimers (Chart 1, right) [15, 16], covalently linked porphyrin-ZnDAP hetero dimers [17], and arylethynyl-ZnDAP [8] were successfully prepared from **2M** (M = Ni, Cu, Zn) using Pd-catalyzed cross- or homo-coupling reactions. These β-functionalized MDAP derivatives show effective π-conjugation between the MDAP rings and the β-substituents. For example, pyrrole-bridged MDAP dimers (M = Ni, Cu) show broad and intense charge-transfer (CT) bands in the range 600–880 nm in CH_2Cl_2 [16]. The electronic and steric properties of the *meso* nitrogen atoms clearly play important roles in producing these characteristic optical and electrochemical properties. Recently, Shinokubo *et al.* also used **1Ni** and **2Ni** to synthesize 3-alkyl-, 3-phenyl-, and 3-(2-pyridyl)-NiDAPs [18, 19]. 3-(2-Pyridyl)-NiDAP acts as an external *N*,*N*-chelating ligand for Pt^{II}, Ru^{II}, and Re^I ions. To the best of our knowledge, however, the number of peripherally functionalized diazaporphyrins is still limited, and the structure-property relationships between the β-aryl substituents and diazaporphyrin π-systems have not been systematically studied. Here we report the first comparative study of a series of 3-aryl-MDAPs **3** and **4** (Ar-MDAPs; Chart 1), which were obtained by Suzuki–Miyaura cross-coupling reactions of **2M** (M = Ni, Zn) with arylboronic acids. The electronic effects of the β-aryl substituents on the optical and electrochemical properties of the entire MDAP π-systems of **3** and **4** are discussed on the basis of experimental and theoretical results.

RESULTS AND DISCUSSION

First, we explored a new protocol for the peripheral functionalization of MDAP rings using Suzuki–Miyaura cross-coupling reactions of **2M** with arylboronic acids (Scheme 1). Br-NiDAP **2Ni**, prepared from **1Ni** and NBS according to the reported procedure [15], was reacted with phenylboronic acid in the presence of $Pd(OAc)_2$ (20 mol%), 2-biphenyldicyclohexylphosphine (CyJohnPhos, 40 mol%), and K_2CO_3 in a dioxane-water mixed solvent at 80 °C. After 2 h, **2Ni** was consumed
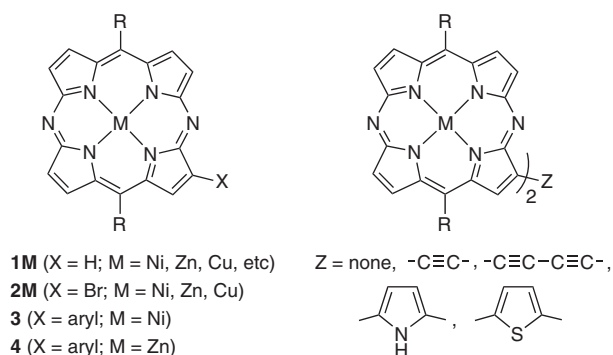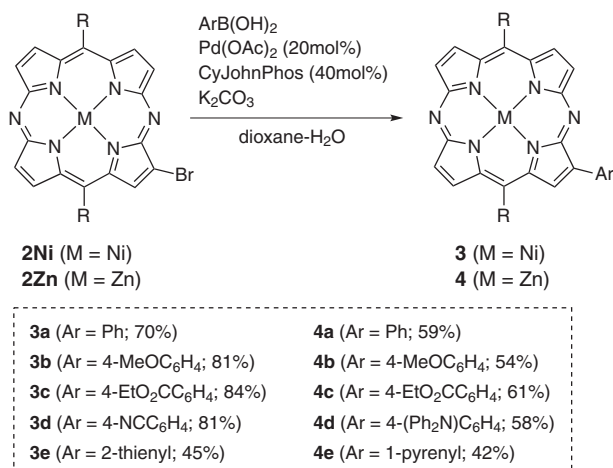

1M (X = H; M = Ni, Zn, Cu, etc)
2M (X = Br; M = Ni, Zn, Cu)
3 (X = aryl; M = Ni)
4 (X = aryl; M = Zn)

Z = none, −C≡C−, −C≡C−C≡C−,

Chart 1. MDAP derivatives **1**–**4** (left) and covalently linked MDAP dimers (right). $R = 2,4,6\text{-}Me_3C_6H_2$

2Ni (M = Ni)
2Zn (M = Zn)

3 (M = Ni)
4 (M = Zn)

3a (Ar = Ph; 70%)	**4a** (Ar = Ph; 59%)
3b (Ar = 4-$MeOC_6H_4$; 81%)	**4b** (Ar = 4-$MeOC_6H_4$; 54%)
3c (Ar = 4-$EtO_2CC_6H_4$; 84%)	**4c** (Ar = 4-$EtO_2CC_6H_4$; 61%)
3d (Ar = 4-NCC_6H_4; 81%)	**4d** (Ar = 4-$(Ph_2N)C_6H_4$; 58%)
3e (Ar = 2-thienyl; 45%)	**4e** (Ar = 1-pyrenyl; 42%)

Scheme 1. Synthesis of **3** and **4**; $R = 2,4,6\text{-}Me_3C_6H_2$. CyJohnPhos = 2-biphenyldicyclohexylphosphine

completely, and silica-gel column chromatography of the reaction mixture afforded Ph-NiDAP **3a** as a purple solid in 70% isolated yield. Shinokubo *et al.* independently prepared **3a** by the reaction of **1Ni** with phenyllithium [19]. The Suzuki–Miyaura cross-coupling strategy was also used for the synthesis of other arylboronic acids, producing Ar-NiDAPs **3b**–**3e** in 45–84% yields. Under the same reaction conditions, Br-ZnDAP **2Zn** underwent cross-coupling reactions with several arylboronic acids to give the corresponding Ar-ZnDAPs **4a**–**4e** in 42–61% yields. The practical advantages of this Suzuki–Miyaura protocol are the relatively short reaction times (1–3 h in most cases) and high functional group tolerances, represented by the syntheses of **3c**, **3d** and **4c**.

Ar-NiDAPs **3** and Ar-ZnDAPs **4** were fully characterized using ¹H NMR spectroscopy and high-resolution mass spectrometry. In the ¹H NMR spectra of **3a**–**3d** and **4a**–**4d**, the *ortho* protons of the β-aryl groups are observed at low fields compared with the *meta/para* protons; this indicates ring-current effects derived from the adjacent MDAP rings. The structure of **3c** was unambiguously determined using X-ray crystallography.
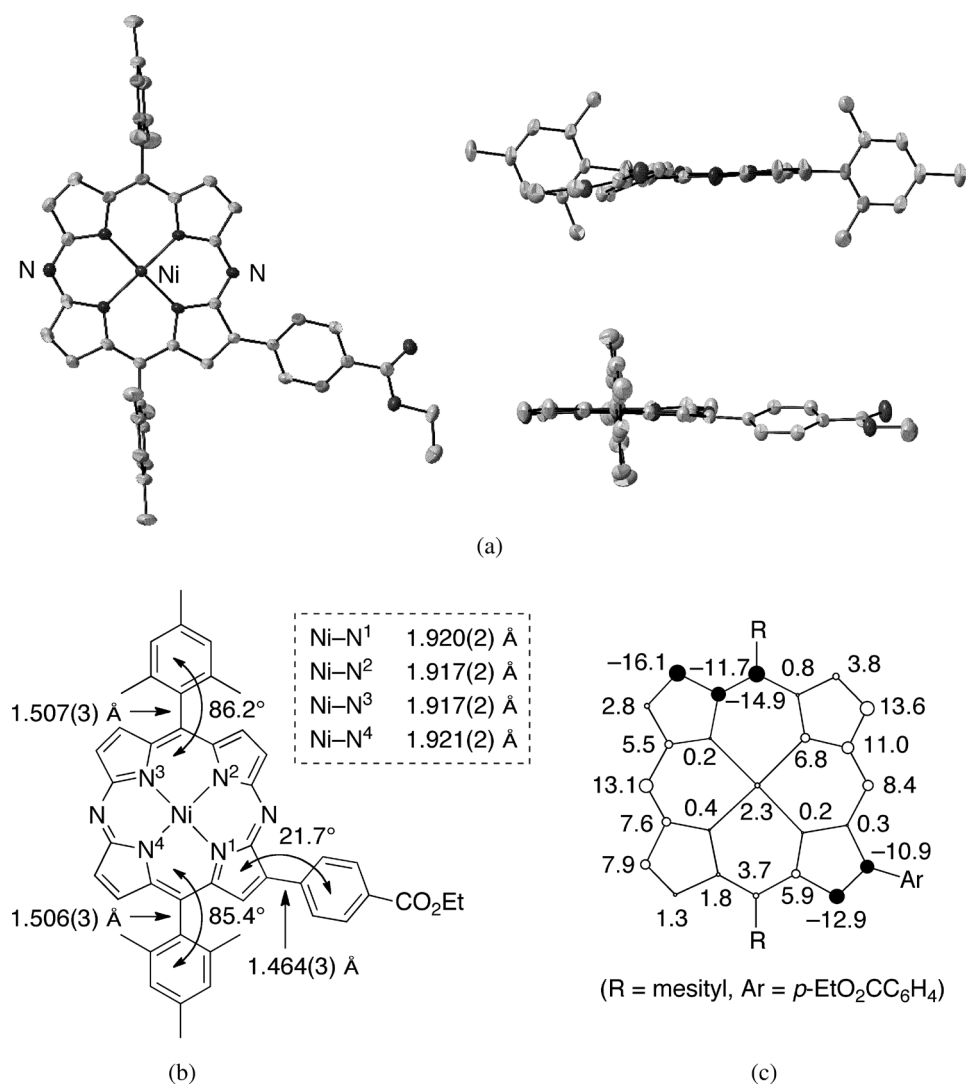
Fig. 1. (a) ORTEP diagrams of **3c** (50% probability ellipsoids). Hydrogen atoms are omitted for clarity. Top (left), side (right, upper), and front (right, lower) views. (b) Selected bond lengths and dihedral angles. (c) Deviations of the 25 atoms from the average NiDAP π-plane (in pm). The sizes of circles correspond to the degrees of deviations

Single crystals of **3c** were grown from toluene-octane. As shown in Fig. 1, the Ni center in **3c** adopts a square planar geometry, with Ni–N bond lengths of 1.917(2)–1.921(2) Å; these are very close to the bond lengths in **3a** [1.912(3)–1.920(3) Å] reported by Shinokubo and coworkers [19]. The DAP π-plane of **3c** is slightly ruffled (root-mean-square of deviation of the 25 atoms from the mean NiDAP π-plane (Δd_{RMS}) = 0.083 Å) compared with the β-unsubstituted NiDAP **1Ni** (Δd_{RMS} = 0.018 Å) [12]. The *meso*-mesityl rings are almost perpendicular to the NiDAP π-plane (the dihedral angles between the two mean planes are 85.4–86.2°), whereas the β-aryl ring leans toward the NiDAP π-plane (dihedral angle = 21.7°). These results are in good accordance with the previously reported results of the crystal structures of **3a** [19] and 3,7,13,17-tetraphenyl-NiDAP [12], in which the β-phenyl groups lean toward the mean NiDAP plane with dihedral angles of 7.8–22.3° and 16.2–34.6°,

respectively. The inter-ring bond length between the NiDAP and β-aryl rings [1.464(3) Å] in **3c** is shorter than those between the NiDAP and *meso*-mesityl rings [1.506(3)–1.507(3) Å]. The results show that the NiDAP ring is conjugated with the β-aryl group much more efficiently than with the *meso*-mesityl group, based on geometric factors. All attempts to grow good-quality single crystals of Ar-ZnDAPs **4** have been unsuccessful.

To gain insights into the structures of Ar-ZnDAPs, we performed density functional theory (DFT) calculations at the B3LYP/6-311G(d,p) level, using two models, **4a–4m** and **4d–4m**, in which the *meso*-mesityl groups were replaced by phenyl groups (Fig. 2). As shown at the bottom of Fig. 2, the *meso*-phenyl groups are significantly twisted against the MDAP π-plane (dihedral angles between the mean planes are 69.8–72.4°) because of steric repulsion between the *ortho*-C–H and pyrrolic β-C–H groups. In contrast, the β-phenyl groups lean
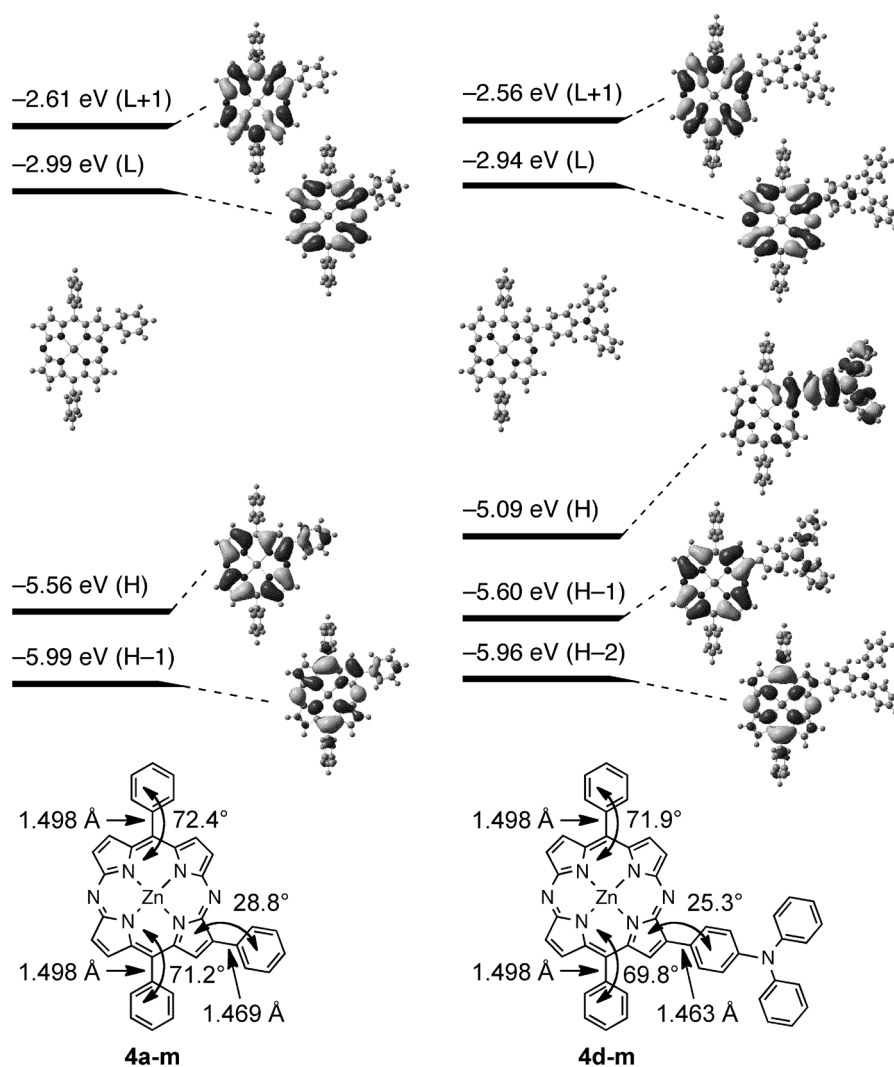
Fig. 2. Orbital diagrams and energies (in eV) at the optimized structures of **4a–m** and **4d–m** calculated at the B3LYP/6-311G(d,p) level. H = HOMO, L = LUMO. Selected bond lengths and dihedral angles are listed in the bottom

toward the MDAP π-plane (dihedral angles = 25.3–28.8°), as the neighboring *meso* nitrogen atom has no substituent. The inter-ring bond lengths between the ZnDAP and β-aryl rings (1.469 Å for **4a–4m**, 1.463 Å for **4d–4m**) are appreciably shorter than those between the ZnDAP and *meso*-phenyl rings (1.498 Å). These geometrical parameters suggest that the β-aryl groups conjugate with the ZnDAP π-system more efficiently than do the *meso*-phenyl groups. The orbitals on the DAP rings of both models are very similar in shape and energy. In contrast, **4d–4m** has a high-lying HOMO that is localized on the *p*-Ph₂NC₆H₄ group. This implies that **4a** and **4d** have different optical and electrochemical properties, derived from their HOMOs (*vide infra*).

The ¹H NMR spectra of Ar-ZnDAPs **4** showed concentration dependence of the chemical shifts of some of the peripheral protons at concentrations above 2 mM. For example, an increase in the concentration of a CDCl₃ solution of **4c** from 2 to 10 mM caused upfield shifts of the

¹H signals of two sets of β-C–H protons ($\Delta\delta$ = 0.61 ppm for H$_a$, H$_{a'}$; $\Delta\delta$ = 0.13 ppm for H$_b$, H$_{b'}$), and this process was reversible (Fig. 3). The other Ar-ZnDAP derivatives showed similar concentration-dependent spectroscopic changes. Electron-spray high-resolution mass spectra of solutions of **4c** showed intense ion peaks attributable to its dimer, [(**4c**)₂ + H]⁺. These results suggest that Ar-ZnDAPs **4** undergo self-aggregation in concentrated solutions to form noncovalently stacked dimers; *i.e.* the upfield shifts of some of the β-C–H protons (H$_a$, H$_{a'}$) are probably caused by ring-current effects of the neighboring ZnDAP ring. This type of concentration dependence of the ¹H NMR chemical shifts was not observed for Ar-NiDAPs **3**, suggesting that the zinc center in **4** plays a key role in the aggregation behavior. Although we do not have any direct evidence for aggregated structures, partially overlapped DAP dimers may be formed by dipole–dipole interactions between the two ZnDAP rings [20, 21] and/or electrostatic interactions between the central zinc and
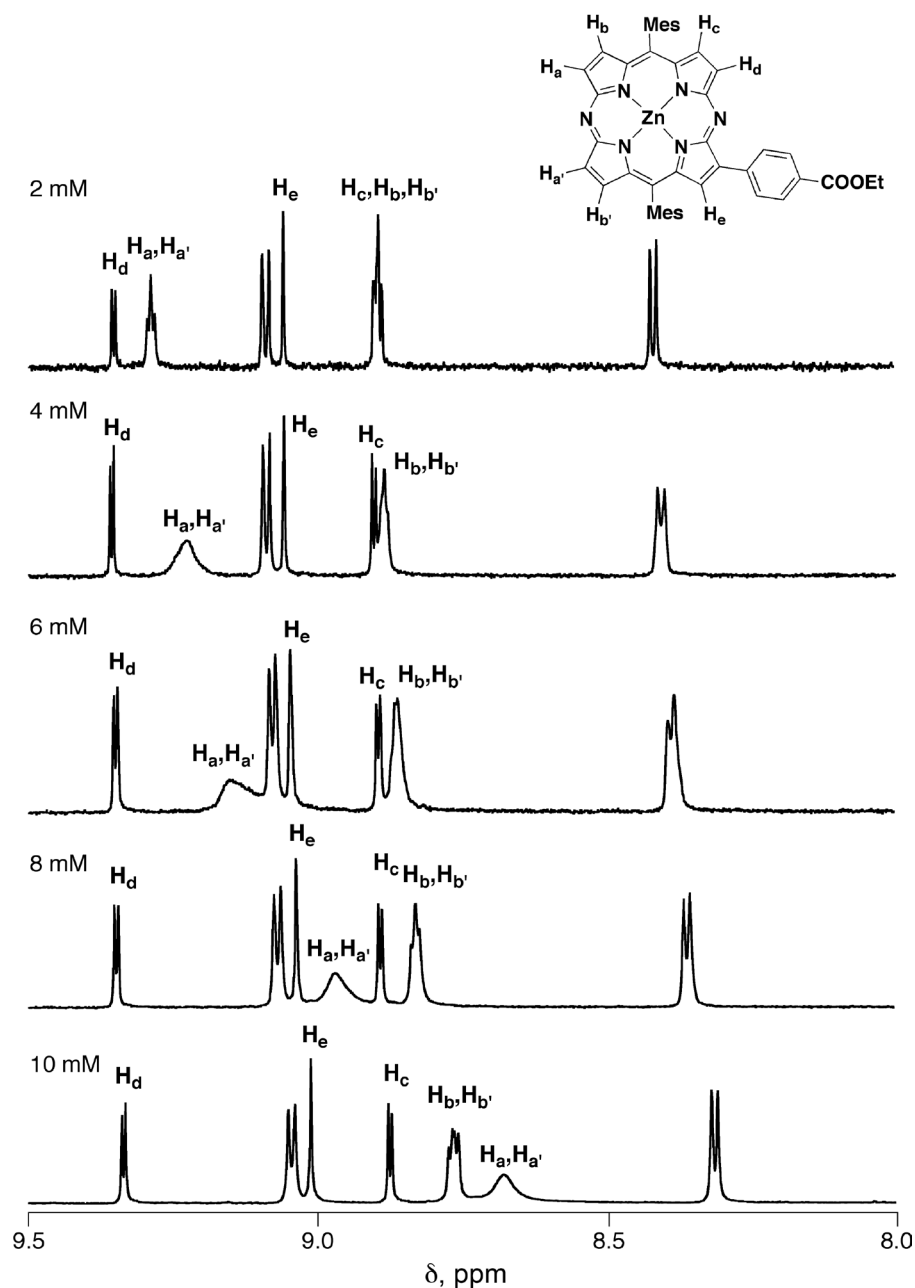
Fig. 3. Concentration dependence of ^{1}H NMR spectra (9.5–8.0 ppm) of **4c** in CDCl$_3$

meso nitrogen atoms. The addition of an excess of CD$_3$OD or pyridine to CDCl$_3$ solutions of **4c**, **4d** suppressed aggregation. The zinc-pyridine binding constants (K) of **4c** and **4d** in CH$_2$Cl$_2$ at 23 °C were determined to be 9.2×10^3 and 1.4×10^4 M^{-1}, respectively, by titration of their absorption spectra. The small difference between the K values indicates that the electronic effects of the *para* substituents on the ligation behavior of ZnDAPs are small.

To clarify the electronic effects of the β-aryl substituents on the optical properties of the MDAP π-systems, UV-visible absorption (for **3** and **4**) and fluorescence (for **4**) spectra were obtained in solutions

(Table 1). At the measurement concentrations ([**4**] $< 1.0 \times 10^{-5}$ M), Ar-ZnDAPs **4** did not undergo self-aggregation and were present as monomers. All the β-arylated MDAPs **3** and **4** showed bathochromically shifted absorption/emission bands relative to those of the β-unsubstituted MDAPs **1Ni** [12] and **1Zn** [14]. Figures 4a and 4b summarize the absorption spectra of **3a–3c**, **3e** and **4a–4c**, **4e**, respectively, in CH$_2$Cl$_2$. The electronic effects of the *p*-methoxy and *p*-ethoxycarbonyl groups on the Soret and Q-bands are small; the absorption maxima of the Q-bands (λ_Q) of **3b**, **3c** and **4b**, **4c** are bathochromically shifted ($\Delta\lambda_Q = 1$–4 nm) from those of the respective phenyl derivatives **3a** and **4a**. The electronic
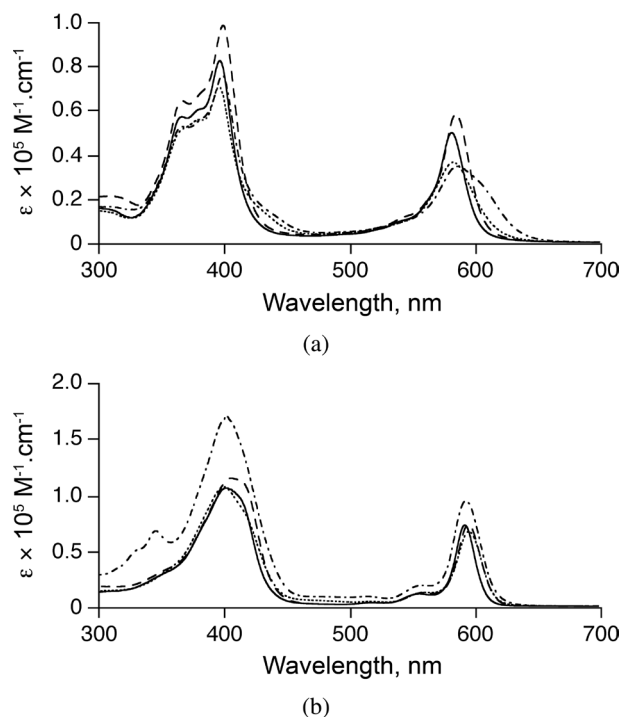
(a)

(b)

Fig. 4. UV-vis absorption spectra of (a) **3a** (solid line), **3b** (dotted line), **3c** (dashed line), and **3e** (chain line) and (b) **4a** (solid line), **4b** (dotted line), **4c** (dashed line), and **4e** (chain line) in CH_2Cl_2

effects of these *para* substituents on the emission maxima (λ_{em}) are also small ($\Delta\lambda_{em}$ = 6–7 nm **4b**, **4c** *vs.* **4a**). The β-(2-thienyl) group causes broadening and a slight red shift of the Q-band ($\Delta\lambda_Q$ = 5 nm **3e** *vs.* **3a**) as a result of π-conjugation. The absorption spectrum of **4e** is basically

a superimposition of those of pyrene and **1Zn**, implying that the β-(1-pyrenyl) group has only a small impact on the electronic transition of the ZnDAP chromophore. A change of the solvent from CH_2Cl_2 to toluene, THF, MeCN, $CHCl_3$, and DMF did not greatly influence the λ_Q/λ_{em} values and Stokes shifts of **4a**–**4c**, suggesting that the polarizabilities of **4a**–**4c** are comparable (Table 2).

The spectroscopic features of p-$Ph_2NC_6H_4$-ZnDAP **4d** are different from those of Ph-ZnDAP **4a** (Fig. 5). Both the Q and emission bands of **4d** are considerably broadened and red-shifted compared with those of **4a**. In addition, the Stokes shift of **4d** ($\Delta\nu = \nu_{abs} - \nu_{em}$ = 3490 cm⁻¹) is much greater than that of **4a** ($\Delta\nu$ = 280 cm⁻¹). The spectroscopic features of **4d** contrast sharply with those of 5-[*p*-(diphenylamino)phenyl]-10,15,20-trimesitylporphyrinatozinc(II) reported by Su and coworkers [22]. This porphyrin shows Q-bands at 551/588 nm and emission bands at 600/648 nm, which are close to the respective values for 5,10,15,20-tetra-mesitylporphyrinatozinc(II) (λ_Q = 550/587 nm; λ_{em} = 592/644 nm). Clearly, a *meso*-(*p*-$Ph_2NC_6H_4$) group has only a small impact on the optical properties of the porphyrin π-system, probably because of the twisted orientation toward the porphyrin ring.

When the solvent was changed from toluene to CH_2Cl_2, the Stokes shifts of **4d** changed from 2060 (in toluene) to 3490 cm⁻¹ (in CH_2Cl_2). The large Stokes shifts and solvatochromism indicate that the entire π-system of **4d** has a pronounced CT character in the excited state. Figure 6 shows the Lippert–Mataga plots [23] of **4d** in the absence or presence of pyridine. In the absence of pyridine, the plot (closed triangles) displays two series

Table 1. Optical and electrochemical data for **3** and **4**[a]

3/4 (Ar)	λ_Q, nm[b]	λ_{em}, nm (Φ_F)	E_{ox}, V[c]	E_{red}, V[c]	ΔE[d]
3a (Ph)	582 (4.70)	n.m.	+0.77	-1.37, -1.81	2.14
3b (4-$MeOC_6H_4$)	583 (4.56)	n.m.	+0.72	-1.37, -1.82	2.09
3c (4-$EtO_2CC_6H_4$)	585 (4.77)	n.m.	+0.80	-1.33, -1.78	2.13
3d (4-$NCCC_6H_4$)	587 (4.74)	n.m.	+0.83	-1.30, -1.77	2.13
3e (2-thienyl)	587 (4.55)	n.m.	+0.69[e]	-1.33, -1.79	2.02
1Ni [f]	571 (4.78)	n.m.	+0.80[e]	-1.40, -2.02	2.20
4a (Ph)	593 (4.86)	603 (0.03)	+0.74[h]	-1.47, -2.04[h]	2.21
4b (4-$MeOC_6H_4$)	597 (4.82)	610 (0.03)	+0.69[h]	-1.47, -2.09[h]	2.16
4c (4-$EtO_2CC_6H_4$)	596 (4.87)	609 (0.03)	+0.76[h]	-1.39, -1.94[h]	2.15
4d (4-$Ph_2NC_6H_4$)	603 (4.88)	764 (0.08)	+0.49, +0.70[h]	-1.43, -1.97[h]	1.92
4e (1-pyrenyl)	594 (4.97)	611 (0.06)	+0.62,[e] +0.81[e]	-1.33, -1.71	1.95
1Zn [g]	584 (4.86)	588 (0.02)	n.m.	n.m.	n.m.

[a] Measured in CH_2Cl_2 unless otherwise noted. n.m. = not measured. [b] Absorption maxima in the range of >500 nm. Data in parentheses are logarithms of extinction coefficients. [c] Oxidation (E_{ox}) and reduction (E_{red}) potentials *vs.* Fc/Fc⁺, determined by CV with Bu_4NPF_6 as a supporting electrolyte. Each process is reversible unless otherwise noted. [d] $\Delta E = E_{ox,1} - E_{red,1}$. [e] Irreversible. [f] Data from [12]. [g] Data from [14]. Measured in CH_2Cl_2–MeOH (1:1 v/v). [h] Measured in THF.
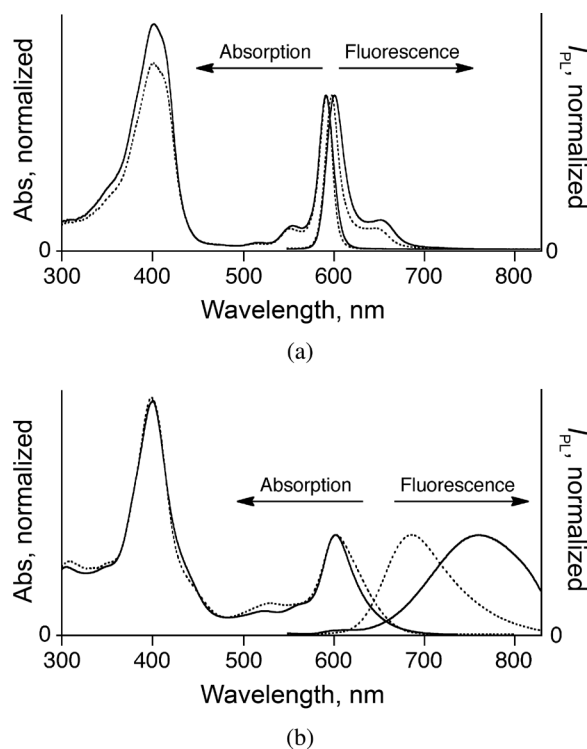
(a)

(b)

Fig. 5. Absorption and fluorescence spectra of (a) **4a** and (b) **4d** in CH_2Cl_2 (solid line) and toluene (dotted line)

of linear solvation energy relationships (LSERs) *vs.* the orientation polarizability (Δf); one series is related to noncoordinating solvents (toluene, $CHCl_3$, and CH_2Cl_2), and the other is related to coordinating solvents (THF, MeCN, and DMF). The solvent molecules of the latter series probably coordinate to the zinc center, which may change the CT character of the DAP π-system to some extent. In the presence of an excess (*ca.* 1000 equiv.) of pyridine, the pyridine-**4d** adduct is formed predominantly in all the solvents, and the plot (open circles) displays a good LSER ($\Delta\nu/\Delta f = 7.3 \times 10^3$ cm^{-1}, $R = 0.98$). It should be noted that the HOMO of **4d–4m** is localized mainly on

the triphenylamine unit, whereas the HOMO of **4a–4m** is located on the ZnDAP ring (Fig. 2). As a result, the HOMO of **4d–4m** is destabilized by 0.47 eV compared with that of **4a–4m**. However, the LUMOs of these two models are located on ZnDAP rings with almost the same orbital energies. It is evident that the strongly electron-donating *p*-diphenylamino group greatly enhances the donor-acceptor interactions between the triphenylamine and ZnDAP units. The difference between the dipole moments of **4a–4m** (0.193 D) and **4d–4m** (1.214 D) supports the intrinsic CT character of the entire π-system of **4d**.

To investigate the electronic effects of the β-aryl substituents on the redox properties of the MDAP π-systems, the oxidation and reduction potentials (E_{ox} and E_{red} *vs.* Fc/Fc$^+$) of **3** and **4** were measured using cyclic voltammetry in CH_2Cl_2 or THF, with Bu$_4$NPF$_6$ as the supporting electrolyte (Table 1). The *para* substituents on the β-aryl groups of **3a–3d** and **4a–4c** have small but distinct electronic effects on the E_{ox} values, which shifted anodically in the orders **3b** (+0.72 V) < **3a** (+0.77 V) < **3c** (+0.80 V) < **3d** (+0.83 V) and **4b** (+0.69 V) < **4a** (+0.74 V) < **4c** (+0.76 V). The E_{ox} value of **4d** (+0.49 V) is greatly shifted to the negative side from that of **4a**. These data basically reflect the resonance effects of the *para* substituents on the electron-donating ability of the Ar-MDAP π-systems. The electronic effects on the E_{red} values are less significant than those on the E_{ox} values ($\Delta E_{red} < 0.07$ V for **3b–3d** *vs.* **3a**; $\Delta E_{red} < 0.08$ V for **4b–4d** *vs.* **4a**). The observed data can be reasonably explained by considering the differences between the orbital coefficients of the β-aryl rings in the HOMOs and LUMOs. As shown in Fig. 2, the HOMOs of **4a–4m** and **4d–4m** have sufficient orbital coefficients on the β-aryl rings, whereas the LUMOs do not. The resonance effects of the *para* substituents on the ZnDAP π-system are more distinct on the HOMO than on the LUMO.

In summary, we prepared a series of 3-aryl-10,20-dimesityl-5,15-diazaporphyrin-metal complexes using Suzuki–Miyaura cross-coupling reactions and examined

Table 2. Solvent effects on the optical data for **4**[a]

	Toluene	THF	CH_3CN	$CHCl_3$	CH_2Cl_2	DMF
4a (Ph)	594, 600 (170)	593, 601 (220)	592, 605 (360)	595, 603 (220)	593, 603 (280)	595, 607 (330)
4b (4-MeOC$_6$H$_4$)	597, 609 (330)	597, 607 (280)	595, 610 (410)	598, 611 (360)	597, 610 (360)	599, 612 (360)
4c (4-EtO$_2$CC$_6$H$_4$)	597, 606 (250)	596, 609 (360)	595, 612 (470)	598, 610 (330)	596, 609 (360)	598, 615 (460)
4d (4-Ph$_2$NC$_6$H$_4$)	604, 689 (2040)	604, 715 (2570)	602, 742 (3130)	606, 736 (2910)	603, 764 (3490)	605, 755 (3280)
4d (4-Ph$_2$NC$_6$H$_4$)[b]	609, 669 (1470)	604, 717 (2610)	602, 778 (3760)	609, 720 (2530)	606, 745 (3080)	606, 754 (3240)

[a] λ_Q (left) and λ_{em} (right) values, in nm. Data in parentheses are Stokes shifts ($\Delta\nu = \nu_Q - \nu_{em}$), in cm^{-1}. [b] Pyridine (*ca.* 1000 equiv.) was added.

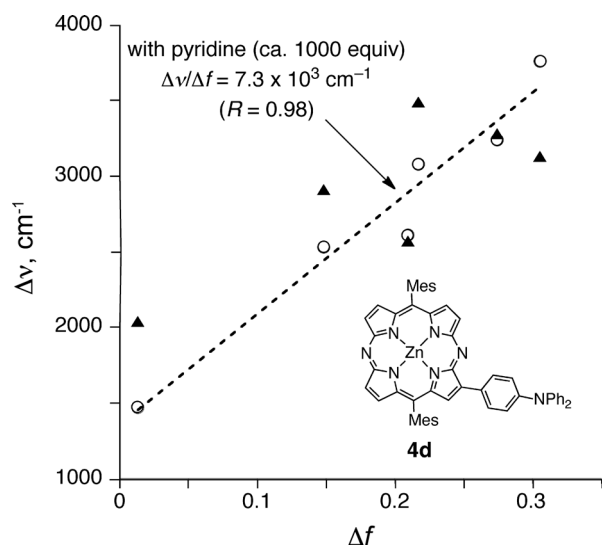**Fig. 6.** Lippert–Mataga plots of **4d**: $\Delta v = v_{abs} - v_{em}$; $\Delta f = (\varepsilon - 1)/(2\varepsilon + 1) - (n^2 - 1)/(2n^2 + 1)$. ε = dielectric constant; n = refractive index. Closed triangles are Stokes shifts (Δv) in the absence of pyridine. Open circles are Stokes shifts in the presence of pyridine (*ca.* 1000 equiv. *vs.* **4d**)

their optical and electrochemical properties. Effective π-conjugation through the inter-ring C–C bond was suggested by the small dihedral angle between the β-aryl group and the NiDAP π-system. The electronic effects of *para* substituents were studied using UV-visible absorption/fluorescence spectroscopy, cyclic voltammetry, and DFT calculations. Among the Ar-ZnDAPs, the *p*-Ph₂N-substituted derivative shows significant donor (triphenylamine)-acceptor (ZnDAP) interactions because of the high-lying HOMO localized on the triphenylamine moiety. This intramolecular CT interaction eventually leads to high visible-light-absorbing ability of the entire π-system. The present results confirm that the introduction of a highly electron-donating aryl group at the peripheral β-carbon would be a promising strategy for constructing MDAP-based visible-NIR-responsive functional dyes.

EXPERIMENTAL

General

All melting points were recorded on a Yazawa micro melting point apparatus and are uncorrected. ¹H NMR spectra were recorded on a Varian 700 MHz spectrometer using $CDCl_3$ or CD_2Cl_2 as a solvent. Chemical shifts are reported as relative values *vs.* tetramethylsilane. High-resolution mass spectra (HRMS) were obtained on a Thermo Fisher Scientific EXACTIVE spectrometer. UV-vis absorption spectra were measured at room temperature on a JASCO V-530 spectrometer. Fluorescence quantum yield measurements were performed on a Hamamatsu

Photonics Quantaurus-QY spectrometer. Electrochemical measurements were performed at room temperature on a CH Instruments model 650E electrochemical workstation using a glassy carbon working electrode, a platinum wire counter electrode, and an Ag/Ag⁺ [0.01 M AgNO₃, 0.1 M Bu₄NPF₆ (MeCN)] reference electrode. Scan rate was 60 mV.s⁻¹, and the potentials were calibrated with ferrocene/ferrocenium (Fc/Fc⁺). Compounds **1M** and **2M** were prepared according to the reported procedures [12, 14, 15]. Other chemicals and solvents were of reagent grade quality and used without further purification unless otherwise noted. Thin-layer chromatography was performed with Alt. 5554 DC-Alufolien Kieselgel 60 F254 (Merck), and preparative column chromatography was performed using Silica Gel 60 spherical, neutrality (Nacalai tesque). All reactions were performed under an argon or nitrogen atmosphere. The synthetic procedures and characterization data of new compounds are described below.

Synthesis and characterization

3-Aryl-5,15-diaza-10,20-dimesitylporphinato-nickel(II) (3). Typical procedure: A mixture of **2Ni** (20.1 mg, 0.029 mmol), Pd(OAc)₂ (1.5 mg, 0.0067 mmol), 2-biphenyldicyclohexylphosphine (4.0 mg, 0.011 mmol), K₂CO₃ (11.7 mg, 0.085 mmol), phenylboronic acid (17.9 mg, 0.147 mmol), 1,4-dioxane (5 mL), and distilled water (0.5 mL) was heated at 80 °C. After 2 h, CH_2Cl_2 and water were added, and the combined organic extracts were separated, washed with brine, dried over Na₂SO₄, and concentrated under reduced pressure to leave a solid residue, which was then chromatographed on silica gel using hexane/AcOEt as eluents. The purple fraction ($R_f = 0.65$ in hexane/AcOEt = 5/1) was collected, concentrated, and recrystallized from CH_2Cl_2/MeOH to give **3a** as a purple solid (14.0 mg, 70%). According to similar procedures, **3b**–**3e** were prepared from **2Ni** and the corresponding arylboronic acids.

3a. [19] mp > 300 °C. ¹H NMR (700 MHz; CDCl₃): δ_H, ppm 1.80 (s, 6H, *ortho*-Me), 1.83 (s, 6H, *ortho*-Me), 2.60 (s, 3H, *para*-Me), 2.62 (s, 3H, *para*-Me), 7.26 (s, 2H, Mes-*meta*), 7.28 (s, 2H, Mes-*meta*), 7.56 (t, *J* = 7.7 Hz, 1H, phenyl) 7.72 (pseudo-t, *J* = 7.7 Hz, 2H, phenyl), 8.77–8.79 (m, 5H, pyrrole-β and phenyl), 8.86 (s, 1H, pyrrole-β), 9.15 (d, *J* = 4.9 Hz, 2H, pyrrole-β), 9.20 (d, *J* = 4.2 Hz, 1H, pyrrole-β). HRMS (ESI): *m/z* 681.2241 (calcd. for [M + H]⁺ 681.2271). UV-vis (CH₂Cl₂): λ_max, nm (log ε) 396 (4.92), 582 (4.70).

3b. ($R_f = 0.42$ in hexane/AcOEt = 5/1) mp > 300 °C. ¹H NMR (700 MHz; CD₂Cl₂): δ_H, ppm 1.81 (s, 6H, *ortho*-Me), 1.83 (s, 6H, *ortho*-Me) 2.62 (s, 3H, *para*-Me), 2.63 (s, 3H, *para*-Me), 3.99 (s, 3H, OMe), 7.26 (d, *J* = 9.1 Hz, 2H, phenyl), 7.30 (s, 2H, Mes-*meta*), 7.31 (s, 2H, Mes-*meta*), 8.75–8.77 (m, 5H, pyrrole-β and phenyl), 8.80 (s, 1H, pyrrole-β), 9.121 (d, *J* = 4.9 Hz, 1H, pyrrole-β), 9.124 (d, *J* = 4.9 Hz, 1H, pyrrole-β), 9.18 (d, *J* = 4.9 Hz,

1H, pyrrole-β). HRMS (ESI): m/z 711.2350 (calcd. for [M + H]$^+$ 711.2377). UV-vis (CH$_2$Cl$_2$): λ_{max}, nm (log ε) 396 (4.85), 583 (4.56).

3c. (R_f = 0.44 in hexane/AcOEt = 5/1) mp > 300 °C. ^{1}H NMR (700 MHz; CDCl$_3$): δ_H, ppm 1.49 (t, J = 7.0 Hz, 3H, -CO$_2$CH$_2$CH_3), 1.81 (s, 6H, *ortho*-Me), 1.84 (s, 6H, *ortho*-Me) 2.61 (s, 3H, *para*-Me), 2.63 (s, 3H, *para*-Me), 4.49 (q, J = 7.0 Hz, 2H, -CO$_2$CH_2CH$_3$), 7.27 (s, 2H, Mes-*meta*), 7.29 (s, 2H, Mes-*meta*), 8.38 (d, J = 8.4 Hz, 2H, phenyl), 8.77 (d, J = 4.9 Hz, 1H, pyrrole-β), 8.78 (d, J = 4.9 Hz, 1H, pyrrole-β), 8.79 (d, J = 4.9 Hz, 1H, pyrrole-β), 8.88 (d, J = 8.4 Hz, 2H, phenyl), 8.94 (s, 1H, pyrrole-β), 9.149 (d, J = 4.9 Hz, 1H, pyrrole-β), 9.153 (d, J = 4.9 Hz, 1H, pyrrole-β), 9.19 (d, J = 4.9 Hz, 1H, pyrrole-β). HRMS (ESI): m/z 753.2474 (calcd. for [M + H]$^+$ 753.2482). UV-vis (CH$_2$Cl$_2$): λ_{max}, nm (log ε) 399 (503), 585 (4.77).

3d. (R_f = 0.48 in hexane/AcOEt = 5/1) mp > 300 °C. ^{1}H NMR (700 MHz; CD$_2$Cl$_2$): δ_H, ppm 1.81 (s, 6H, *ortho*-Me), 1.83 (s, 6H, *ortho*-Me) 2.62 (s, 3H, *para*-Me), 2.63 (s, 3H, *para*-Me), 7.30 (s, 2H, Mes-*meta*), 7.31 (s, 2H, Mes-*meta*), 8.01 (d, J = 8.4 Hz, 2H, phenyl), 8.78 (d, J = 4.9 Hz, 1H, pyrrole-β), 8.786 (d, J = 4.9 Hz, 1H, pyrrole-β), 8.787 (d, J = 4.9 Hz, 1H, pyrrole-β), 8.986 (d, J = 8.4 Hz, 2H, phenyl), 8.987 (s, 1H, pyrrole-β), 9.137 (d, J = 4.9 Hz, 1H, pyrrole-β), 9.142 (d, J = 4.9 Hz, 1H, pyrrole-β), 9.19 (d, J = 4.9 Hz, 1H, pyrrole-β). HRMS (ESI): m/z 706.2215 (calcd. for [M + H]$^+$ 706.2224). UV-vis (CH$_2$Cl$_2$): λ_{max}, nm (log ε) 400 (4.97), 587 (4.74).

3e. (R_f = 0.47 in hexane/AcOEt = 5/1) mp > 300 °C; ^{1}H NMR (700 MHz; CDCl$_3$): δ_H, ppm 1.81 (s, 6H, *ortho*-Me), 1.83 (s, 6H, *ortho*-Me) 2.61 (s, 3H, *para*-Me), 2.64 (s, 3H, *para*-Me), 7.27 (s, 2H, Mes-*meta*), 7.29 (s, 2H, Mes-*meta*), 7.36 (dd, J = 3.5, 4.9 Hz, 1H, thienyl-β), 7.69 (dd, J = 1.4, 4.9 Hz, 1H, thienyl-α), 8.47 (dd, J = 1.4, 3.5 Hz, 1H, thienyl-β 8.73 (d, J = 4.9 Hz, 1H, pyrrole-β), 8.760 (s, 1H, pyrrole-β), 8.761 (d, J = 4.9 Hz, 1H, pyrrole-β), 8.77 (d, J = 4.9 Hz, 1H, pyrrole-β), 9.118 (d, J = 4.9 Hz, 1H, pyrrole-β), 9.122 (d, J = 4.9 Hz, 1H, pyrrole-β), 9.21 (d, J = 4.9 Hz, 1H, pyrrole-β). HRMS (ESI): m/z 687.1821 (calcd. for [M + H]$^+$ 687.1835). UV-vis (CH$_2$Cl$_2$): λ_{max}, nm (log ε) 398 (4.89), 587 (4.55).

3-Aryl-5,15-diaza-10,20-dimesitylporphinato-zinc(II) (4). Typical procedure: A mixture of **2Zn** (26.9 mg, 0.039 mmol), Pd(OAc)$_2$ (1.6 mg, 0.007 mmol), 2-biphenyldicyclohexylphosphine (5.5 mg, 0.016 mmol), K$_2$CO$_3$ (15.7 mg, 0.114 mmol), 4-(ethoxycarbonyl) phenylboronic acid (37.6 mg, 0.194 mmol), 1,4-dioxane (6 mL), and distilled water (0.6 mL) was heated at 80 °C. After 1.5 h, CH$_2$Cl$_2$, pyridine, and water were added, and the combined organic extracts were separated, washed with brine several times, dried over Na$_2$SO$_4$, and concentrated under reduced pressure to leave a solid residue, which was then chromatographed on silica gel using CH$_2$Cl$_2$/AcOEt/pyridine as eluents. The green fraction (R_f = 0.48 in CH$_2$Cl$_2$/AcOEt = 100/5) was collected, concentrated, and recrystallized from CH$_2$Cl$_2$/MeOH to give **4c** as

a purple solid (18.0 mg, 61%). According to similar procedures, **4a**, **4b**, **4d**, **4e** were prepared from **2Zn** and the corresponding arylboronic acids.

4a. (R_f = 0.13 in CH$_2$Cl$_2$/AcOEt = 100/1) mp > 300 °C. ^{1}H NMR (700 MHz; CDCl$_3$/CD$_3$OD): δ_H, ppm 1.86 (s, 6H, *ortho*-Me), 1.88 (s, 6H, *ortho*-Me), 2.65 (s, 3H, *para*-Me), 2.67 (s, 3H, *para*-Me), 7.31 (s, 2H, Mes-*meta*), 7.33 (s, 2H, Mes-*meta*), 7.58 (t, J = 7.0 Hz, 1H, phenyl), 7.76 (pseudo-t, J = 7.0 Hz, 2H, phenyl), 8.81–8.82 (m, 3H, pyrrole-β), 8.85 (d, J = 7.0 Hz, 2H, phenyl), 8.88 (s, 1H, pyrrole-β), 9.16 (d, J = 4.2 Hz, 1H, pyrrole-β), 9.17 (d, J = 4.2 Hz, 1H, pyrrole-β), 9.26 (d, J = 4.2 Hz, 1H, pyrrole-β). HRMS (ESI): m/z 686.2197 (calcd. for [M + H]$^+$ 687.2209). UV-vis (CH$_2$Cl$_2$): λ_{max}, nm (log ε) 402 (5.02), 593 (4.86).

4b. (R_f = 0.77 in CH$_2$Cl$_2$/MeOH = 50/1) mp > 300 °C. ^{1}H NMR (700 MHz; CD$_2$Cl$_2$, 2 mM): δ_H, ppm 1.85 (s, 6H, *ortho*-Me), 1.87 (s, 6H, *ortho*-Me), 2.65 (s, 3H, *para*-Me), 2.66 (s, 3H, *para*-Me), 4.02 (s, 3H, OMe), 7.309 (s, 2H, Mes-*meta*), 7.310 (d, J = 8.4 Hz, 2H, phenyl), 7.32 (s, 2H, Mes-*meta*), 8.87–8.89 (m, 4H, pyrrole-β), 8.99 (d, J = 8.4 Hz, 2H, phenyl), 9.29 (d, J = 4.2 Hz, 1H, pyrrole-β), 9.30 (d, J = 4.2 Hz, 1H, pyrrole-β), 9.35 (d, J = 4.2 Hz, 1H, pyrrole-β). HRMS (ESI): m/z 717.2300 (calcd. for [M + H]$^+$ 717.2315). UV-vis (CH$_2$Cl$_2$): λ_{max}, nm (log ε) 400 (5.03), 597 (4.82).

4c. (R_f = 0.48 in CH$_2$Cl$_2$/AcOEt = 20/1) mp > 300 °C. ^{1}H NMR (700 MHz; CDCl$_3$, 1 mM): δ_H, ppm 1.14 (t, J = 6.7 Hz, 3H, -CO$_2$CH$_2$CH_3), 1.85 (s, 6H, *ortho*-Me), 1.87 (s, 6H, *ortho*-Me), 2.65 (s, 3H, *para*-Me), 2.67 (s, 3H, *para*-Me), 4.50 (q, J = 6.7 Hz, 2H, -CO$_2$CH_2CH$_3$), 7.31 (s, 2H, Mes-*meta*), 7.34 (s, 2H, Mes-*meta*), 8.42 (d, J = 8.0 Hz, 2H, phenyl), 8.89–8.90 (m, 3H, pyrrole-β), 9.06 (s, 1H, pyrrole-β), 9.09 (d, J = 8.0 Hz, 2H, phenyl), 9.30 (d, J = 4.2 Hz, 1H, pyrrole-β), 9.31 (d, J = 4.2 Hz, 1H, pyrrole-β), 9.35 (d, J = 4.2 Hz, 1H, pyrrole-β). HRMS (ESI): m/z 759.2409 (calcd. for [M + H]$^+$ 759.2420). UV-vis (CH$_2$Cl$_2$): λ_{max}, nm (log ε) 406 (5.06), 596 (4.87).

4d. (R_f = 0.58 in CH$_2$Cl$_2$/AcOEt/pyridine = 100/1/1) mp 248 °C (decomposed). ^{1}H NMR (700 MHz; CD$_2$Cl$_2$/ CD$_3$OD): δ_H, ppm 1.85 (s, 6H, *ortho*-Me), 1.88 (s, 6H, *ortho*-Me), 2.64 (s, 3H, *para*-Me), 2.65 (s, 3H, *para*-Me), 7.13 (t, J = 7.4 Hz, 2H, phenyl-*para*), 7.28 (d, J = 7.4 Hz, 4H, phenyl-*ortho*), 7.33 (s, 2H, Mes-*meta*), 7.34 (s, 2H, Mes-*meta*), 7.37 (pseudo-t, J = 7.4 Hz, 4H, phenyl-*meta*), 7.42 (d, J = 8.8 Hz, 2H, phenylene), 8.77 (d, J = 4.2 Hz, 1H, pyrrole-β), 8.78 (d, J = 4.2 Hz, 1H, pyrrole-β), 8.79 (d, J = 4.2 Hz, 1H, pyrrole-β), 8.81 (s, 1H, pyrrole-β), 8.84 (d, J = 8.8 Hz, 2H, phenylene), 9.15 (d, J = 4.2 Hz, 1H, pyrrole-β), 9.17 (d, J = 4.2 Hz, 1H, pyrrole-β), 9.22 (d, J = 4.2 Hz, 1H, pyrrole-β). HRMS (ESI): m/z 854.2931 (calcd. for [M + H]$^+$ 854.2944). UV-vis (CH$_2$Cl$_2$): λ_{max}, nm (log ε) 304 (4.71), 401 (5.25), 603 (4.88).

4e. (R_f = 0.36 in CH$_2$Cl$_2$/AcOEt = 100/1) mp 281–282 °C (decomposed). ^{1}H NMR (700 MHz; CD$_2$Cl$_2$/ CD$_3$OD): δ_H, ppm 1.85 (s, 6H, *ortho*-Me), 1.98 (s, 6H, *ortho*-Me), 2.60 (s, 3H, *para*-Me), 2.63 (s, 3H, *para*-Me),

7.32 (s, 2H, Mes-*meta*), 7.33 (s, 2H, Mes-*meta*), 8.03 (d, $J = 8.4$ Hz, 1H, pyrenyl), 8.09 (pseudo-t, $J = 8.4$ Hz, 1H, pyrenyl), 8.22 (d, $J = 8.4$ Hz, 1H, pyrenyl), 8.27 (d, $J = 8.4$ Hz, 1H, pyrenyl), 8.32 (m, 2H, pyrenyl), 8.57 (d, $J = 8.4$ Hz, 1H, pyrenyl), 8.59 (d, $J = 8.4$ Hz, 1H, pyrenyl), 8.74 (d, $J = 4.2$ Hz, 1H, pyrrole-β), 8.82 (d, $J = 4.2$ Hz, 1H, pyrrole-β), 8.87 (d, $J = 4.2$ Hz, 1H, pyrrole-β), 8.91 (d, $J = 8.4$ Hz, 1H, pyrenyl), 9.04 (d, $J = 4.2$ Hz, 1H, pyrrole-β), 9.06 (s, 1H, pyrrole-β), 9.21 (d, $J = 4.2$ Hz, 1H, pyrrole-β), 9.23 (d, $J = 4.2$ Hz, 1H, pyrrole-β). HRMS (ESI): *m/z* 811.2505 (calcd. for [M + H]$^+$ 811.2522). UV-vis (CH$_2$Cl$_2$): λ_{max}, nm (log ε) 278 (4.69), 348 (4.82), 400 (5.22), 594 (4.97).

X-ray crystallographic analysis

Single crystals of **3c** were grown from toluene-octane. All measurements were made on a Rigaku Mercury70 diffractometer using multi-layer mirror monochromated Mo-Kα radiation. (0.71070 Å) at 150 K. The data were corrected for Lorentz and polarization effects. The structures were solved by using direct methods (SIR2008) and refined by full-matrix least squares techniques against F^2 using SHELXL97 [24]. The non-hydrogen atoms were refined anisotropically, and hydrogen atoms were refined using the rigid model. **3c**. C$_{45}$H$_{38}$N$_6$NiO$_2$, MW = 753.53, $0.20 \times 0.20 \times 0.10$ mm, triclinic, *P*–1, $a = 8.2136$ (10) Å, $b = 13.000$ (2) Å, $c = 18.011$ (3) Å, $\alpha = 110.379$ (4)°, $\beta = 90.037$ (3)°, $\gamma = 97.249$ (3)°, $V = 1786.3$ (5) Å^3, $Z = 2$, $\rho_{calcd} = 1.401$ g.cm^{-3}, $\mu = 5.93$ cm^{-1}, collected 20110, independent 8898, parameters 487, $R_w = 0.1627$ (all data), $R_1 = 0.0597$ ($I > 2.0\sigma(I)$), GOF = 1.104.

Computational details

The geometries of the model compounds were optimized using the DFT method. The basis sets used were 6-311G(d,p) basis set [25] for H, C, and N and the Wachters–Hay all electron basis set [26] supplemented with one *f*-function (exponent: 1.62) for Zn. The functional of DFT was the Becke, three-parameter, Lee–Yang–Parr (B3LYP) exchange-correlation functional [27]. We confirmed that the optimized geometries were not in saddle but in stable points. All the calculations were carried out using the Gaussian 09 suite of programs [28].

Supporting information

Crystallographic data for **3c** have been deposited at the Cambridge Crystallographic Data Centre (CCDC) under number CCDC-1048127. Copies can be obtained on request, free of charge, *via* www.ccdc.cam.ac.uk/data_request/cif or from the Cambridge Crystallographic Data Centre, 12 Union Road, Cambridge CB2 1EZ, UK (fax: +44 1223-336-033 or email: data_request@ccdc.cam.ac.uk).

REFERENCES

1. Kobayashi N. In *The Porphyrin Handbook,* Vol. 2, Kadish KM, Smith KM and Guilard R. (Eds.) Academic Press: San Diego, CA, 2000; pp 301–360.
2. Mack J and Kobayashi N. *Chem. Rev.* 2011; **111**: 281.
3. Ogata H, Fukuda T, Nakai K, Fujimura Y, Neya S, Stuzhin PA and Kobayashi N. *Eur. J. Inorg. Chem.* 2004; 1621.
4. Pan N, Bian Y, Yokoyama M, Li R, Fukuda T, Neya S, Jiang J and Kobayashi N. *Eur. J. Inorg. Chem.* 2008; 5519.
5. Mack J, Sosa-Vargas L, Coles SJ, Tizzard GJ, Chambrier I, Cammidge AN, Cook MJ and Kobayashi N. *Inorg. Chem.* 2012; **51**: 12820.
6. Andrianov DS, Rybakov VB and Cheprakov AV. *Chem. Commun.* 2014; **50**: 7953.
7. Shinmori H, Kodaira F, Matsugo S, Kawabata S and Osuka A. *Chem. Lett.* 2005; **34**: 322.
8. Kurotobi K, Kawamoto K, Toude Y, Fujimori Y, Kinjo Y, Ito S, Matano Y and Imahori H. *Chem. Lett.* 2013; **42**: 725.
9. Borisov SM, Zenkl G and Klimant I. *ACS Appl. Mater. Interfaces* 2010; **2**: 366.
10. Yamamoto M, Takano Y, Matano Y, Stranius K, Tkachenko NV, Lemmetyinen H and Imahori H. *J. Phys. Chem. C* 2014; **118**: 1808.
11. Horie M, Hayashi Y, Yamaguchi S and Shinokubo H. *Chem. Eur. J.* 2012; **18**: 5919.
12. Matano Y, Shibano T, Nakano H and Imahori H. *Chem. Eur. J.* 2012; **18**: 6208.
13. The synthesis of β-substituted DAPs using a templating method was reported earlier: (a) Harris RLN, Johnson AW and Kay IT. *J. Chem. Soc. C* 1966; 22. (b) Khelevina OG, Chizhova NV, Stuzhin PA, Semeikin AS and Berezin BD. *Russ. J. Coord. Chem.* 1997; **71**: 74.
14. Matano Y, Shibano T, Nakano H, Kimura Y and Imahori H. *Inorg. Chem.* 2012; **51**: 12879.
15. Matano Y, Fujii D, Shibano T, Furukawa K, Nakano H, Higashino T and Imahori H. *Chem. Eur. J.* 2014; **20**: 3342.
16. Omomo S, Maruyama Y, Furukawa K, Furuyama T, Nakano H, Kobayashi N and Matano Y. *Chem. Eur. J.* 2015; **21**: 2003.
17. Abou-Chahine F, Fujii D, Imahori H, Nakano H, Tkachenko NV, Matano Y and Lemmetyinen H. *J. Phys. Chem. B* ASAP (DOI: 10.1021/jp510903a).

18. Yamaji A, Shin JY, Miyake Y and Shinokubo H. *Angew. Int. Ed. Engl.* 2014; **53**: 13924.

19. Yamaji A, Hiroto S, Shin JY and Shinokubo H. *Chem. Commun.* 2013; **49**: 5064.

20. Hunter CA and Sanders JKM. *J. Am. Chem. Soc.* 1990; **112**: 5525.

21. Hunter CA. *Chem. Soc. Rev.* 1994; 101.

22. Huang CY, Hsu CY, Yang LY, Lee CJ, Yang TF, Hsu CC, Ke CH and Su YO. *Eur. J. Inorg. Chem.* 2012; 1038.

23. Lakowicz JR. *Principles of Fluorescence Spectroscopy*, 3rd ed., Springer: Berlin, 2006.

24. Sheldrick GM. *Acta Cryst.* 2008; **A64**: 112.

25. Krishnan R, Binkley JS, Seeger R and Pople JA. *J. Chem. Phys.* 1980; **72**: 650.

26. (a) Wachters AJH. *J. Chem. Phys.* 1970; **52**: 1033. (b) Hay PJ. *J. Chem. Phys.* 1977; **66**: 4377. (c) Raghavachari K and Trucks GW. *J. Chem. Phys.* 1989; **91**: 1062.

27. (a) Becke AD. *J. Chem. Phys.* 1993; **98**: 5648. (b) Lee C, Yang W and Parr RG. *Phys. Rev. B* 1988; **37**: 785.

28. Frisch MJ, Trucks GW, Schlegel HB, Scuseria GE, Robb MA, Cheeseman JR, Scalmani G, Barone V, Mennucci B, Petersson GA, Nakatsuji H, Caricato M, Li X, Hratchian HP, Izmaylov AF, Bloino J, Zheng G, Sonnenberg JL, Hada M, Ehara M, Toyota K, Fukuda R, Hasegawa J, Ishida M, Nakajima T, Honda Y, Kitao O, Nakai H, Vreven T, Montgomery, Jr. JA, Peralta JE, Ogliaro F, Bearpark M, Heyd JJ, Brothers E, Kudin KN, Staroverov VN, Keith T, Kobayashi R, Normand J, Raghavachari K, Rendell A, Burant JC, Iyengar SS, Tomasi J, Cossi M, Rega N, Millam JM, Klene M, Knox JE, Cross JB, Bakken V, Adamo C, Jaramillo J, Gomperts R, Stratmann RE, Yazyev O, Austin AJ, Cammi R, Pomelli C, Ochterski JW, Martin RL, Morokuma K, Zakrzewski VG, Voth GA, Salvador P, Dannenberg JJ, Dapprich S, Daniels AD, Farkas O, Foresman JB, Ortiz JV, Cioslowski J and Fox DJ. *Gaussian 09, Revision B.01*; Gaussian, Inc., Wallingford CT, 2010.